ACS OMEGA

http://pubs.acs.org/journal/acsodf

Article

# Nanocatalyst-Assisted Facile One-Pot Synthesis of Glycidol from Glycerol and Dimethyl Carbonate

Elrasheed Elhaj, Huajun Wang,* Mohd Imran,* Salah Eldeen F Hegazi, Mohamed Hassan, Mubarak A Eldoma, Jabir Hakami, Waseem A. Wani, and Anis Ahmad Chaudhary

Cite This: *ACS Omega* 2022, 7, 31778−31788

Read Online

ACCESS | Metrics & More | Article Recommendations

**ABSTRACT:** This paper reports the facile one-pot synthesis of glycidol via the transesterification of glycerol with dimethyl carbonate using $KNO_3/Al_2O_3$ nanoparticles as supporting catalysts. $KNO_3/Al_2O_3$ nanoparticles were prepared by the impregnation method. XRD and FT-IR analyses indicated an interaction between $KNO_3$ and $Al_2O_3$ that enabled the decomposition of $KNO_3$ during the process and resulted in the formation of $KAl_5O_8$, the Al−O−K group, and $K_2O$. $K_2O$ was recognized as one of the active sites of the catalyst. SEM results indicated the high performance of the supporting catalyst, as the catalytic activity depended on both the number of catalytic active sites and their distribution. The yield of glycidol was 64% at the expense of 95% glycerol under moderate reaction conditions (120 min, 1 atm, and 70 °C). The nanocatalyst prepared at 800 °C with a loading amount of 30% $KNO_3$ was the most efficient for the synthesis of glycidol. Furthermore, the catalyst was recovered and reused without a loss of efficiency even after the fourth recycling. A plausible mechanism for the one-pot synthesis of glycidol has also been proposed.

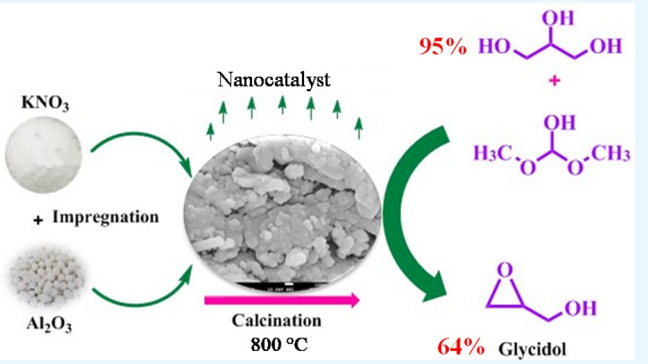


## 1. INTRODUCTION

The past decade has witnessed significant research in the area of biodiesel production.[1−5] As a promising alternative for petroleum, biodiesel has great potential for the energy industry and the green chemical industry. Glycerol (GL) is produced in huge quantities during the production of biodiesel, which has led to decreases in the prices of both biodiesel and purified GL.[6,7] Several researchers have documented the use of heterogeneous, homogeneous, and ionic liquid catalysts for the conversion of GL to value-added chemicals, such as glycerol carbonate (GC) and glycidol (GD).[8−10] Large-scale applications of these materials have been attributed to their unique properties such as low volatility, biodegradability, and low toxicity. GD (2,3-epoxy-1-propanol) is a template for the production of functional epoxides and can be used both in epoxy resins and as a monomer for the synthesis of polymers, diluents, plastics, and fiber modifiers. Owing to its chemical versatility and the well-investigated reactivity of its hydroxyl functional group, GD is expected to serve as a precursor for the design and synthesis of a variety of useful derivatives.[11−13] GD can be prepared through various pathways depending on the type of substrates, such as carbonates, allyl alcohols, and halohydrins, among others.[14−17] Dimethyl carbonate (DMC) is a methylating agent. It plays important roles in transesterification reactions. Traditionally, it is produced by the reaction of phosgene and methanol. The other synthetic routes toward DMC preparation include the oxidative carbonylation of methanol, the transesterification of ethylene carbonate and propylene carbonate, the reaction between carbon monoxide and nitric oxide, and the reaction between $CO_2$ and methanol.[18,19]

Nowadays, the manufacturing process for producing GD for commercial purposes is carried out via the epoxidation of an allyl alcohol, which is a much less environmentally friendly route. Additionally, the process has high production costs and a low efficiency and needs to be carried out under harsh reaction conditions. Moreover, the synthesis of GD produces large amounts of waste in the form of salt and liquid, which need proper treatment before disposal. These disadvantages have tempted researchers to develop new methods for the synthesis of GD. Until now, some homogeneous and heterogeneous catalysts such as tetraethylammonium amino acid ionic liquid, KF/sepiolite, tetramethylammonium hydrox-

Received: April 16, 2022
Revised: June 30, 2022
Accepted: July 5, 2022
Published: August 29, 2022





https://doi.org/10.1021/acsomega.2c02381
*ACS Omega* 2022, 7, 31778−31788

Scheme 1. Synthesis of GD from GL and DMC over the $KNO_3/Al_2O_3$ Solid Base Catalyst

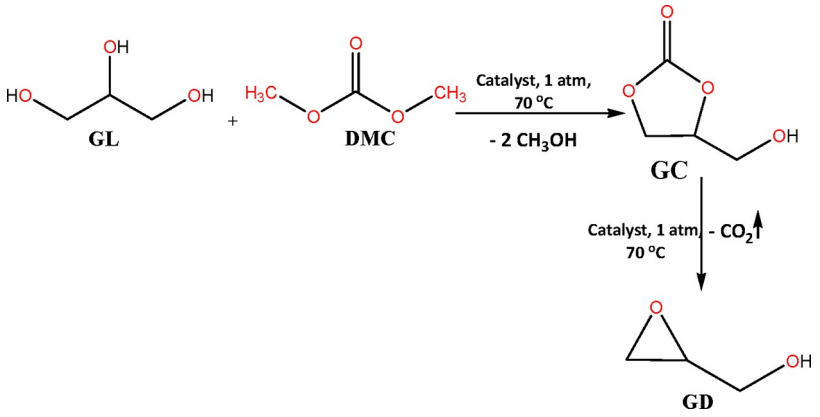


ide ionic liquid, and $NaAlO_2$, have been used for the one-pot synthesis of GD from GL and DMC.[11,12,20] Recently, several one-pot syntheses of GD from GL and DMC were reported.[9,11,12,20−22] Zhou and co-workers reported 79% GD production through 96% conversion of GL using tetraethylammonium pipecolinate ([N2222][Pipe]).[9] The results were manifested using density functional theory (DFT), which suggested the excellent performance of the carboxyl group in ([N2222][Pipe]) ensuring an effective substrate activation. Previously, Lu and co-workers reported a GL conversion and a GC yield of 95.39% and 90.57%, respectively, for the fresh $CaO/Al_2O_3$ catalyst.[23] Even after the fifth recycling of the catalyst, the GL conversion and GC yield were 65.47% and 62.53%, respectively. Additionally, Elhaj and co-workers have reported 87.6% GD production with 96.2% GL conversion using one of the prepared series of functionalized quaternary ammonium salt ionic liquids (FQAILs).[24] Among the FQAILs employed for GD production, the highest conversion was achieved for the hydroxyl group-containing FQAILs. Overall, ionic liquids are too expensive to be used widely in industrial applications. Besides, the separation of ionic liquids from reaction mixtures is often challenging due to their homogeneity. Bai and co-workers reported 94.7% GL conversion with 80.7% GD selectivity using a cheap and easily processed $NaAlO_2$ solid base catalyst under optimum reaction conditions.[11] The process is favored for GD synthesis due to the catalytic efficiency of $NaAlO_2$ along with its tolerance toward water and carbon dioxide. Algoufi and co-workers reported the one-pot synthesis of GD via the transesterification of GL with DMC, which resulted in 99% GL conversion and 82.3% GD synthesis when 30% KF/sepiolite was used as the catalyst.[12] Unfortunately, KF/sepiolite is not an environmentally benign catalyst due to easy loss of $F^-$ ions, which often leads to equipment corrosion and environmental pollution. $CO_2$ has been an important substrate in the preparation of cyclic carbonates, and the formation of cyclic carbonates is a very important part of GD production.[25] Recently, ruthenium-based macromolecules have also been suggested as potential catalysts for GD production in heterogeneous and homogeneous phases that utilize $CO_2$.[26] Overall, there is still an urgent need to design and develop novel and highly efficient heterogeneous catalysts for the one-pot synthesis of GD.

$KNO_3/Al_2O_3$ has been successfully used as a solid base catalyst in transesterification reactions for the production of biodiesel.[27,28] As compared to other solid base catalysts, $KNO_3/Al_2O_3$ does not show any strong basicity prior to activation; thus, the contamination of $CO_2$ from the atmosphere could be avoided, which would simplify the preparation and storage of $KNO_3/Al_2O_3$. In the *in situ* activation process, strong basic sites are formed on the composites due to the decomposition of loaded $KNO_3$. The process also ensures the retention of the high efficiency of the composites.[29−33] To the best of our knowledge, there is no accurate report on the synthesis of GD using $KNO_3/Al_2O_3$ as a catalyst. Therefore, the present work is an effort toward the one-pot synthesis of GD via the transesterification of GL with DMC using nanoparticulate $KNO_3/Al_2O_3$ as a solid base catalyst. X-ray diffraction (XRD), Fourier transform infrared (FT-IR) spectroscopy, scanning electron microscopy (SEM), Brunauer−Emmet−Teller (BET) surface areas and pore volumes, and carbon dioxide-temperature-programmed desorption ($CO_2$-TPD) were used to characterize the prepared catalyst. All parameters affecting the yield in the synthesis of GD were studied in detail. Additionally, attempts were made to propose a plausible mechanism for the one-pot synthesis.

## 2. EXPERIMENTAL SECTION

**2.1. Chemicals.** Potassium nitrate ($KNO_3$), activated aluminum oxide ($Al_2O_3$), GL, and methanol (99% purity) were obtained from Sinopharm Chemical Reagent Co., Ltd., China. GC (90% purity) was procured from Tokyo Chemical Industry Co., Ltd., Japan. GD (97% purity) was purchased from Shanghai SaEn Chemical Technology Co., Ltd., China. Tetraethylene glycol (99% purity) and DMC (99% purity) were procured from Tianjin Guangfu Fine Chemical Research Institute, China. *n*-Butanol (99% purity) was purchased from Shanghai Zhanyun Chemical Co., Ltd., China. Nitrogen gas (99.999% purity) was procured from Sichuan Tianyi Science & Technology Co., Ltd., Sichuan, China.

**2.2. Preparation of the $KNO_3/Al_2O_3$ Solid Base Catalyst.** The $KNO_3/Al_2O_3$ solid base catalyst was prepared via the impregnation method by reacting an aqueous solution of $KNO_3$ with activated $Al_2O_3$ powder. $Al_2O_3$ powder with a surface area of 223.97 $m^2/g$ was used as a supporting material. First, 10.0 g of activated $Al_2O_3$ powder with a grain diameter of 4 mm was dried at 100 °C in an oven for 3 h. The dried $Al_2O_3$ powder was ground using mortar and pestle and sieved using a standard 100 mesh sieve shaker to obtain a fine powder. To prepare the aqueous solution, 3.0 g of $Al_2O_3$ powder and 2.74 g of $KNO_3$ were mixed in a flask in 10 mL of distilled water, and the reaction mixture was stirred for 10 min. The mixture was left for 24 h at ambient temperature and then dried further at


https://doi.org/10.1021/acsomega.2c02381
ACS Omega 2022, 7, 31778−31788

100 °C for 3 h. Consequently, the obtained solid powder was ground further, sieved through a 100 mesh sieve shaker, calcined at 800 °C for 5 h in a muffle furnace with a heating ramp of 5 °C/min. The thus-obtained final products (solid base catalysts) were denoted as $KNO_3/Al_2O_3$ ($n$%, $m$), where $n$ % indicated the amount of $KNO_3$ in percent and $m$ indicated the calcination temperature.

**2.3. Reaction Procedure.** The chemical equation for the one-pot synthesis of GD from GL and DMC is shown in Scheme 1. To a 50 mL three-neck round-bottom flask fitted with a reflux condenser on a magnetic stirrer was added the $KNO_3/Al_2O_3$ solid base catalyst along with a sampling device and a thermometer (accuracy of ±0.1 °C). The reaction mixture was heated at a constant temperature in an oil bath. In each run of the experiment, the concentrations of the catalyst, GL, and DMC were taken in a fixed specific amount in the flask and the heating was specified at a particular temperature. The reaction mixture was heated for 2 h with a constant stirring speed of 600 rpm. The final reaction mixture was centrifuged to regenerate the catalyst, and the filtrate was sampled for further analysis.

**2.4. Catalyst Characterization.** The prepared catalyst was characterized by XRD. To determine the phase and crystallinity of the catalyst, an X'Pert PRO instrument with Cu K$\alpha$ radiation was used at 30 kV and 15 mA over a 2$\theta$ range of 10−80°, with a step size of 0.0167° and a scanning speed of 8 $min^{-1}$. SEM was performed using a TESCAN VEGA3 (20 kV accelerating voltage) microscope to obtain the morphology of the catalyst. To investigate the chemical bonding and functional groups, FT-IR spectra were recorded using a Bruker VERTEX 70 FT-IR spectrometer with a resolution of 2 $cm^{-1}$ over the 400−4000 $cm^{-1}$ wavenumber range. BET surface areas and volumes were determined from the nitrogen adsorption−desorption isotherm, which was generated using the Mircromeritics ASAP 2420 systemat 77 K. The pore volume was given at $p/p_0$ = 0.99. The Barrett−Joyner−Halenda (BJH) method was used to determine the pore size distribution. $CO_2$-TPD studies were performed using a Huasi DAS-7000 apparatus equipped with a thermal conductivity detector to study the basicity of the catalyst. For this, a 100 mg of the catalyst sample was heated to 300 °C for 1 h with a ramp rate of 10 °C/min under a $N_2$ flow of 30 mL/min. After the sample was cooled to room temperature, a 50 mL/min flow of $CO_2$ was introduced into reactor for 1 h. The catalyst was swept with $N_2$ for 30 min to remove physisorbed $CO_2$ from its surface, and the $CO_2$-TPD studies were performed between 90 and 850 °C in the presence of $N_2$ gas. The desorbed $CO_2$ was detected using gas chromatography (Fuli 9790-II).

**2.5. Product Analysis.** All the samples were analyzed by using gas chromatograph outfitted with a capillary column (DM-FFAP) with a length of 30 m and an inner diameter of 0.25 mm in addition to a flame ionization detector (FID). The gas chromatography of the samples was performed on the basis of the internal standard method. For the determination of DMC, GD, and methanol, $n$-butanol was used as the internal standard. For the determination of GC and GL, tetraethylene glycol was used as the internal standard. Nitrogen gas with a flow rate of 40 mL/min was used as a carrier at 0.3 MPa. The injector and detector temperatures were set at 250 and 270 °C, respectively. The column temperature was programmed to have a 2 min initial hold at 70 °C, a heating ramp of 15 °C/min from 70−250 °C, and then a 15 min hold at 250 °C. Good separation peaks (Figure 1) were achieved at the set conditions for all the components in the reaction mixture.

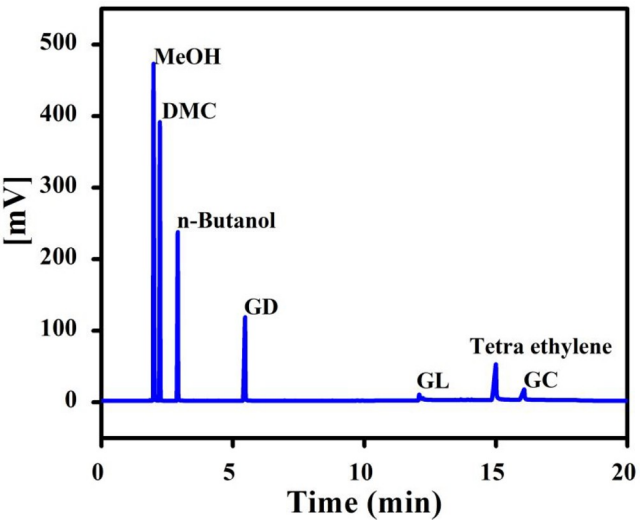


**Figure 1.** Gas chromatogram of the reaction mixture for the synthesis of GD from GL and DMC using $KNO_3/Al_2O_3$ (30%, 800) as the catalyst. Peaks are as follows: (1) methanol, (2) DMC, (3) $n$-butanol, (4) GD, (5) GL;, (6) tetraethylene glycol, and (7) GC.

The conversion of GL ($X_{GL}$), the yield of GD ($Y_{GD}$), and the yield of GC ($Y_{GC}$) were calculated using eqs 1−3, respectively, while the selectivity of GD ($S_{GD}$) was calculated using the eq 4.

$$X_{GL} = \frac{n_{GL}^{in} - n_{GL}^{out}}{n_{GL}^{in}} \times 100\% \quad (1)$$

$$Y_{GD} = \frac{n_{GD}^{out}}{n_{GL}^{in}} \times 100\% \quad (2)$$

$$Y_{GC} = \frac{n_{GC}^{out}}{n_{GL}^{in}} \times 100\% \quad (3)$$

$$S_{GD} = \frac{n_{GD}^{out}}{n_{GL}^{in} - n_{GL}^{out}} \times 100\% \quad (4)$$

Here $n_{GL}^{in}$ is the initial mole number (mol) of GL and $n_{GL}^{out}$, $n_{GD}^{out}$, and $n_{GC}^{out}$ are the mole numbers (mol) of GL, GD, and GC in the residual reaction mixture, respectively.

## 3. RESULTS AND DISCUSSION

**3.1. Effect of the $KNO_3$ Loading Amount and the Calcination Temperature.** A series of $KNO_3/Al_2O_3$ catalysts with various loading amounts of $KNO_3$ over $Al_2O_3$ were prepared and used to catalyze the transesterification of GL with DMC under moderate reaction conditions (DMC/GL molar ratio of 2:1, reaction temperature of 70 °C, reaction time of 120 min, and catalyst amount of 5 wt % based on weight of GL). As shown in Table 1, increasing in the loading amount of $KNO_3$ from 15 wt % to 30 wt % enhanced GL conversion slightly from 94.03% to 95.12%, respectively, and the GD yield increased from 40.50% to 63.52%. As the amount of $KNO_3$ further increased from 30 wt % to 80 wt %, GL conversion decreased from 95.12% to 92.03%, respectively, and the GD yield decreased from 63.52% to 28.78%. Besides, when the loading amount of $KNO_3$ increased from 15 wt % to 80 wt %,


https://doi.org/10.1021/acsomega.2c02381
ACS Omega 2022, 7, 31778−31788

**Table 1. Catalytic Performances of $KNO_3/Al_2O_3$ Solid Base Catalysts in the Transesterification of GL with DMC for the Synthesis of GD at First Use[a]**

| catalyst | $W$ (wt %)[b] | $T_{cal}$ (°C)[c] | $X_{GL}$ (%) | $Y_{GD}$ (%) | $Y_{GC}$ (%) | $S_{GD}$ (%) |
|---|---|---|---|---|---|---|
| $KNO_3/Al_2O_3$ (15%, 800) | 15 | 800 | 94.03 | 40.50 | 53.53 | 43.07 |
| $KNO_3/Al_2O_3$ (30%, 800) | 30 | 800 | 95.12 | 63.52 | 31.60 | 66.78 |
| $KNO_3/Al_2O_3$ (40%, 800) | 40 | 800 | 93.50 | 41.96 | 51.54 | 44.88 |
| $KNO_3/Al_2O_3$ (50%, 800) | 50 | 800 | 88.48 | 32.02 | 56.46 | 36.19 |
| $KNO_3/Al_2O_3$ (80%, 800) | 80 | 800 | 92.03 | 28.78 | 63.25 | 31.27 |
| $KNO_3/Al_2O_3$ (30%, 500) | 30 | 500 | 68.62 | 12.87 | 55.75 | 18.76 |
| $KNO_3/Al_2O_3$ (30%, 600) | 30 | 600 | 87.61 | 29.51 | 58.10 | 33.68 |
| $KNO_3/Al_2O_3$ (30%, 700) | 30 | 700 | 91.58 | 53.62 | 37.96 | 58.55 |
| $KNO_3/Al_2O_3$ (30%, 900) | 30 | 900 | 90.27 | 39.71 | 50.56 | 43.99 |

[a]Reaction conditions are as follows: a DMC/GL molar ratio of 2:1, a reaction temperature of 70 °C, a reaction time of 120 min, and a catalyst amount of 5 wt % based on the weight of GL. [b]Loading amount of $KNO_3$. [c]Calcination temperature.

the GD yield first decreased from 53.53% to 31.60% and the increased to 63.25%. On the contrary, GD selectivity first increased from 43.07% to 66.78% and then decreased to 31.27%. These results suggested that the 30 wt % amount of $KNO_3$ was optimum for the synthesis of GD.

$KNO_3/Al_2O_3$ catalysts with a loading amount of 30 wt % $KNO_3$ were prepared at different calcination temperatures. The data in Table 1 show that increasing the calcination temperature from 500 to 800 °C remarkably increased both the GL conversion and GD yield from 68.62% and 12.87% to 95.12% and 63.52%, respectively. Meanwhile, the GC yield decreased from 55.75% to 31.60%. However, a further increase in the calcination temperature to 900 °C decreased the GL conversion and GD yield to 90.27% and 39.71%, respectively, while the GC yield increased to 50.56%. Besides, it was also observed that the GD selectivity reached the maximum value of 66.78% at 800 °C. Thus, 800 °C was set as the optimized calcination temperature.

XRD patterns of the catalysts $KNO_3/A_2O_3$ (30%, 700−900) were recorded and are depicted in Figure 2a. A new species, namely, rhombohedral $KAl_5O_8$ with a crystalline phase (at $2\theta$ = 15.9°, 20.4°, 32.1°, 35.8°, 41.7°, 45.7°, 57.8°, 62.6°, and 66.8° (JCPDS no. 00-021-0618)), appeared for all the samples. , This phase might have been formed by the interaction of $KNO_3$ with supporter $Al_2O_3$ thus indicating that $K^+$ was successfully loaded into the $Al_2O_3$ framework. A hexagonal $K_2O$ phase (at $2\theta$ = 11.8°, 28.5°, 41.9°, and 57.7° (JCPDS no. 00-026-1327)), which might have been formed by the decomposition of $KNO_3$ at the surface of $Al_2O_3$, also appeared in $KNO_3/A_2O_3$ (30%, 800) and $KNO_3/A_2O_3$ (30%, 700). Interestingly, the peak for the $K_2O$ species was weak and not found for $KNO_3/A_2O_3$ (30%, 900), which suggested that the

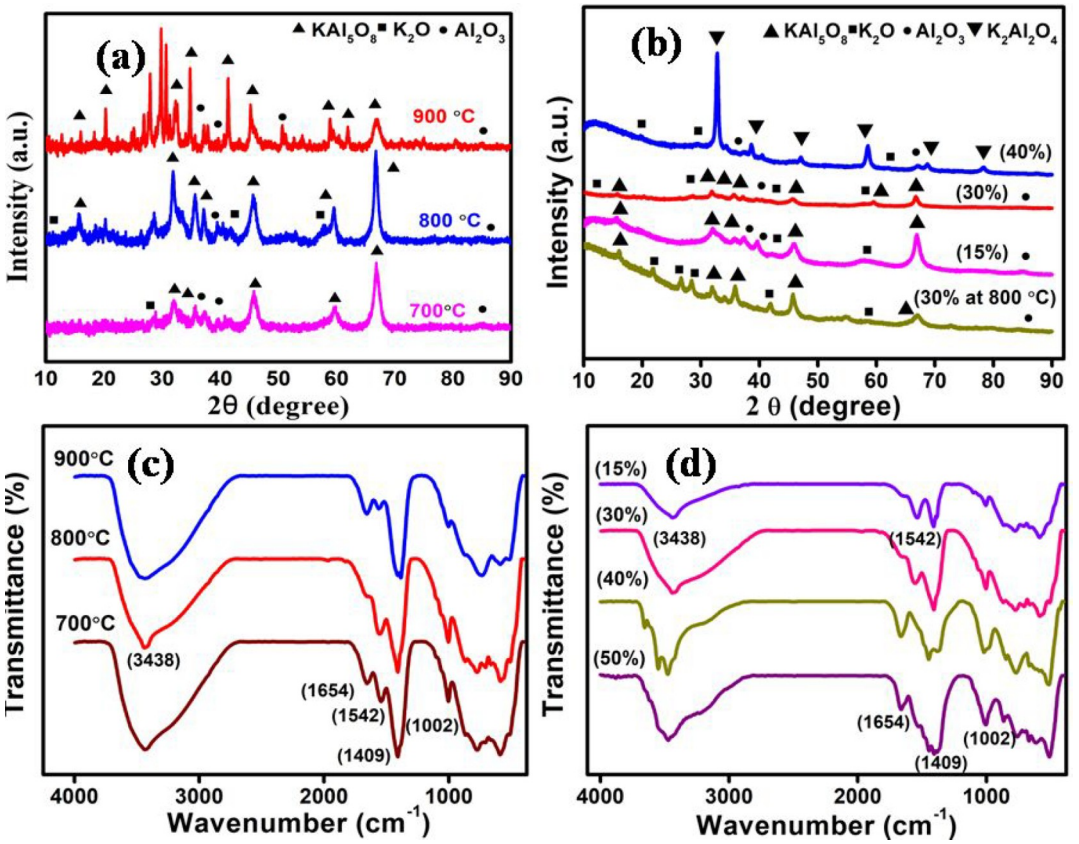


**Figure 2.** (a) XRD patterns of 30% $KNO_3/Al_2O_3$ catalysts at different calcination temperatures. (b) XRD patterns of $KNO_3/Al_2O_3$ catalysts with different loadings (%) of $KNO_3$ at 800 °C and the recovered sample after the second recycling. (c) FT-IR spectra of $KNO_3/Al_2O_3$ at different calcination temperatures. (d) FT-IR spectra of $KNO_3/Al_2O_3$ catalysts with different loadings (%) of $KNO_3$ at 800 °C.



https://doi.org/10.1021/acsomega.2c02381
ACS Omega 2022, 7, 31778−31788

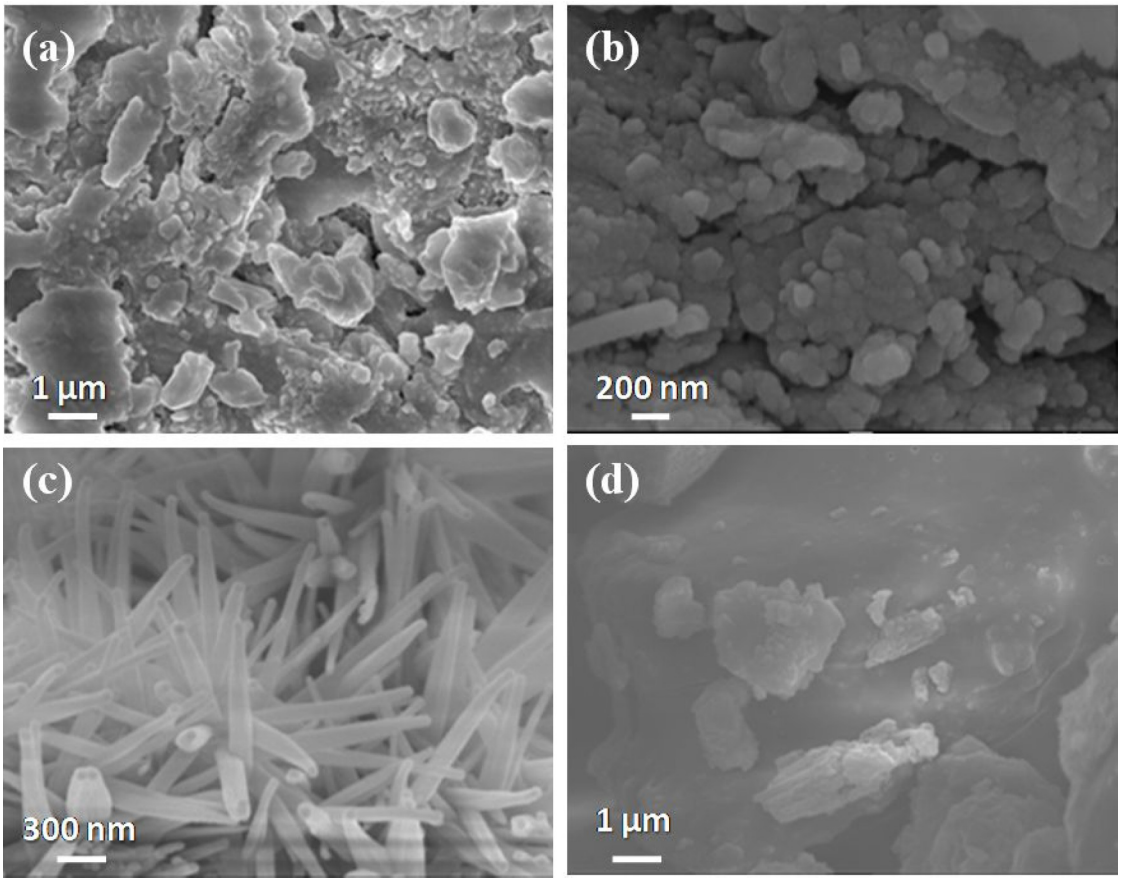


**Figure 3.** SEM images of $KNO_3/Al_2O_3$ catalysts. (a) $KNO_3/Al_2O_3$ (30%, 700), (b) $KNO_3/Al_2O_3$ (30%, 800), (c) $KNO_3/Al_2O_3$ (30%, 900), and (d) $KNO_3/Al_2O_3$ (30%, 800) recovered after the second recycling.

$K_2O$ species was well-dispersed on surface of $Al_2O_3$. Furthermore, the cubic $Al_2O_3$ phase (at $2\theta$ = 37.5°, 39.9°, 50.6°, and 84.9° (JCPDS no. 00-002-1420)) was also observed in the prepared catalysts. The relative content of the $K_2O$ phase in each sample was compared by analyzing of diffraction intensities of the characteristic peaks at $2\theta$ = 28.5° assigned to $K_2O$ in the XRD patterns. The results showed that the relative content of $K_2O$ increased in the pattern in the order $KNO_3/Al_2O_3$ (30%, 800) > $KNO_3/Al_2O_3$ (30%, 700) > $KNO_3/Al_2O_3$ (30%, 900), which is the same as the order for the catalytic activity (Table 1). This indicated that $K_2O$ was one of the active sites for the transesterification of GL with DMC. Figure 2b shows the XRD patterns of $KNO_3/Al_2O_3$ catalysts with different loading amounts of $KNO_3$. For $KNO_3/Al_2O_3$ (15%, 800) and $KNO_3/Al_2O_3$ (30%, 800), the main phases also contained $K_2O$, $Al_2O_3$, and $KAl_5O_8$. However, for $KNO_3/Al_2O_3$ (40%, 800), a new cubic $K_2Al_2O_4$ phase (at $2\theta$ = 32.8°, 38.6°, 47.1°, 58.5°, 68.7°, and 78.3° (JCPDS no 00−045−0849)) was also observed apart from the $K_2O$ and $Al_2O_3$ phases. This new phase might have been formed by the interaction of $KNO_3$ with supporter $Al_2O_3$.

Zhu and co-workers reported the dispersion $KNO_3$ over $Al_2O_3$ at 600 °C.[32] When a certain amount of $KNO_3$ was loaded over $Al_2O_3$ below the monolayer dispersion threshold, a fine dispersion was achieved and strong basic sites were generated at evacuation temperatures above 600 °C. Thus, their finding is consistent with our assumption that the decomposition of $KNO_3$ takes place completely at high calcination temperatures, resulting in high basicity and thus confirming complete decomposition of $KNO_3$. Consequently, the formation of $K_2O$ with new cubic phase $K_2Al_2O_4$ takes place at 40% $KNO_3$. This might be attributed to the intensive interactions between $KNO_3$ and $Al_2O_3$. The amount of $KNO_3$ might be diminished at higher calcination temperature (800 °C) due to either volatilization or a solid−solid reaction, leading to the formation of $KAl_5O_8$ or the penetration of $KNO_3$ into the subsurface.

Figure 2c shows the FT-IR spectra of $KNO_3/Al_2O_3$ catalysts with different calcination temperatures. In all the $KNO_3/Al_2O_3$ catalysts, the absorption band at 1409 $cm^{-1}$ was attributed to the N−O vibration of the nitrate ion ($NO_3^-$). It was found that the band at 1409 $cm^{-1}$ became weaker as the calcination temperature increased from 700−900 °C, indicating the decomposition of $KNO_3$ and the formation of $K_2O$ at higher calcination temperatures. Interestingly, the band does not disappear completely at higher calcination temperature (900 °C), which suggests that $KNO_3$ does not decompose fully at such high temperatures. The peaks at 1654 $cm^{-1}$ in the samples suggested the presence of physisorbed water molecules. The bands at 1542 and 1002 $cm^{-1}$ indicated the presence of carbonate species, which may have been formed by the reaction of basic sites (such as $K_2O$) with $CO_2$ under ambient conditions during the FT-IR analysis. For all samples, the broad band at 3438 $cm^{-1}$ might be partly attributed to the stretching vibrations of Al−O−K groups. The Al−O−K groups might have been formed by $K^+$ ions replacing the protons of the surface hydroxyl groups of alumina.[34] It was important to note that no peaks of K−OH (at 3741 $cm^{-1}$) and


https://doi.org/10.1021/acsomega.2c02381
ACS Omega 2022, 7, 31778−31788

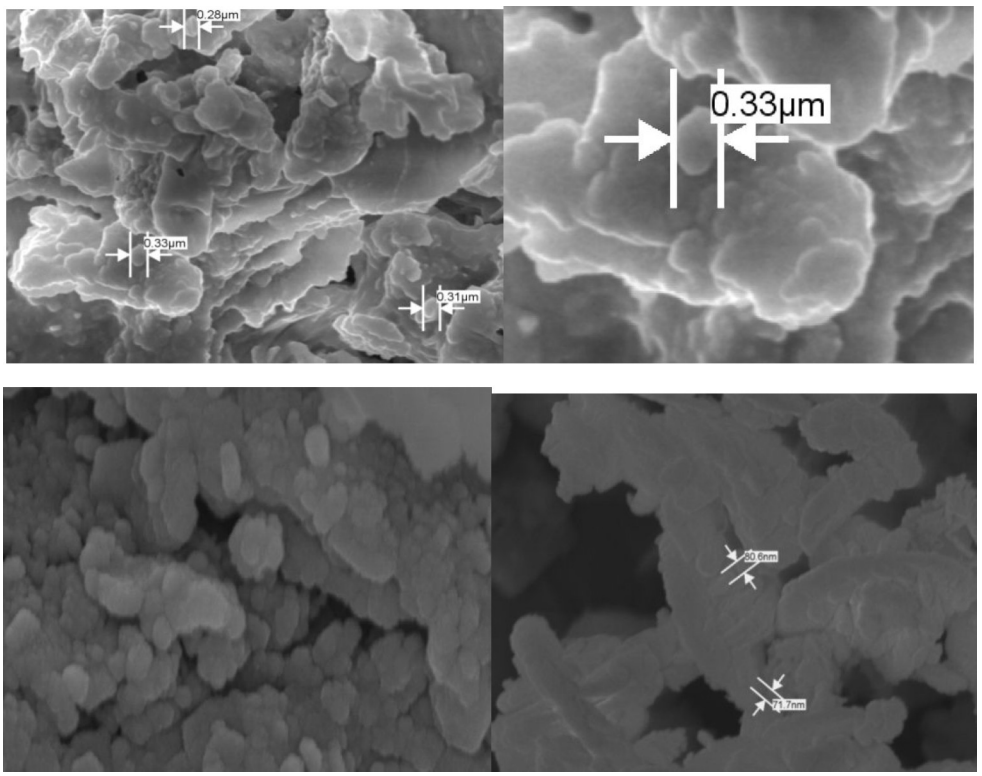


**Figure 4.** SEM images of $KNO_3/Al_2O_3$ (30% $KNO_3$, 800). Images are magnified 10 000−50 000×. Particle size s are 200−300 nm.

$NO_2^-$ species (at 1550 and 1320 $cm^{-1}$) were present in the spectra of the samples, which indicated that neither KOH nor $KNO_2$ was the decomposition product of $KNO_3$. Thus, the $K_2O$ species was deter,omed to be the decomposition product of $KNO_3$ at 700−900 °C, which is consistent with XRD results.

Figure 2d shows the FT-IR spectra of $KNO_3/Al_2O_3$ catalysts with different $KNO_3$ loading amounts. It was observed that the peak at 1409 $cm^{-1}$ caused by the vibration of the N−O bome of nitrate became stronger as the $KNO_3$ loading amount increased, suggesting that the amount of the undecomposed $KNO_3$ increases with the loading amount. Thus, there must be an optimum loading amount of $KNO_3$. Meanwhile, the intensity of the peak at 1002 $cm^{-1}$, which has been attributed to the carbonate species, became stronger as the $KNO_3$ loading amount increased. The bands at 3438 $cm^{-1}$ were attributed to the stretching vibrations of the Al−O−K group. The band at 1654 $cm^{-1}$ was assigned to the physisorbed water, and this band intensified as the $KNO_3$ loading amount increased. Interestingly, no characteristic peaks for $NO_2^-$ and K−OH were detected in the spectra of the samples, which indicated that $KNO_2$ and KOH were not the decomposition products of $KNO_3$. The overall results of the XRD and FT-IR studies indicated that the interaction between the $KNO_3$ phase and the $Al_2O_3$ support, and the decomposition of bulk $KNO_3$, occurred during the preparation of the $KNO_3/Al_2O_3$ catalysts, which resulted in the formation of $KAl_5O_8$, the Al−O−K group, and the $K_2O$ species.

Figure 3 shows the SEM images of the $KNO_3/Al_2O_3$ catalysts. It can be seen from the images that the calcination temperature has an obvious effect on the morphology of the catalyst particles. At calcination temperatures of 700 and 800 °C, the catalysts $KNO_3/Al_2O_3$ (30%, 700) and $KNO_3/Al_2O_3$ (30%, 800) (Figure 3a and b, respectively) underwent the aggregation of particles with various shapes and sizes. The shapes of the nanoparticles resembled cobblestones, with a diameter of about 100 nm. Importantly, at calcination temperature of 900 °C, the $KNO_3/Al_2O_3$ (30%, 900) (Figure 3c) particles were needle-shaped had diameters of about 200−300 nm. The SEM results further indicated that $KNO_3/Al_2O_3$ (30%, 800) was a suitable nanoparticulate catalyst, as higher GD yields were obtained with it.

The catalytic performance of the supported heterogeneous catalysts is greatly influenced by the particle sizes and shapes of the active phase. As a result of this fact, it was observed that the catalytic effect of the $KNO_3/Al_2O_3$ nanoparticles depended on their size and morphology. Additionally, the catalytic performance was dependent on both the nature of the specific interactions between $KNO_3$ and $Al_2O_3$ and the nature and distribution of the active sites under high-temperature sintering. In addition, a new phase ($KAl_5O_8$) and the Al−O−K group are the other components responsible for the activity of the catalyst. Figure 4 shows the magnified SEM image of $KNO_3/Al_2O_3$ (30% $KNO_3$, 800 °C). Additionally, the existence of a new-phase consisting of needle-shaped particles with average particle diameters of 80−200 nm revealed that the high calcination temperature led to a reduction in particle size along with the integration of the active sites.

Table 2 lists the BET surface areas, pore volumes, and pore diameters of the $KNO_3/Al_2O_3$ catalysts. $Al_2O_3$ has a high BET surface area, a large pore volume, and a small pore diameter. On the other hand, the $KNO_3/Al_2O_3$ catalyst has a very low surface area, a small pore volume, and a large pore diameter, indicating that the $K_2O$ active species are well dispersed on $Al_2O_3$ support. In comparison to $KNO_3/Al_2O_3$ (30%, 900), the surface area and pore volume of $KNO_3/Al_2O_3$ (30%, 800) are larger, which is more advantageous for the reaction of GL with DMC.



https://doi.org/10.1021/acsomega.2c02381
ACS Omega 2022, 7, 31778−31788

**Table 2. BET Surface Area, Pore Volume, and Pore Diameter of the $KNO_3/Al_2O_3$ Catalysts**

| sample | BET surface area ($m^2/g$) | pore volume ($cm^3/g$) | pore diameter (nm) |
|---|---|---|---|
| $Al_2O_3$ | 223.97 | 0.4054 | 6.62 |
| $KNO_3/Al_2O_3$ (30%, 800) | 5.90 | 0.0514 | 37.33 |
| $KNO_3/Al_2O_3$ (30%, 900) | 3.83 | 0.0379 | 41.13 |

**Table 3. Basic Properties of $KNO_3/Al_2O_3$ Catalysts**

| | $CO_2$ adsorption peaks (area%) | | | |
|---|---|---|---|---|
| catalyst | ~250 °C | ~390 °C | ~568 °C | total $CO_2$ adsorption (mmol/g) |
| $KNO_3/Al_2O_3$ (30%, 700) | 57 | 36 | 7 | 1.02 |
| $KNO_3/Al_2O_3$ (30%, 800) | 25 | 42 | 33 | 1.38 |
| $KNO_3/Al_2O_3$ (30%, 900) | 72 | 13 | 15 | 1.21 |

$CO_2$ desorption peaks are used in the interpretation of the relationship between the strength of the base and the calcination temperature. Figure 5a shows the $CO_2$-TPD profiles of the $KNO_3/Al_2O_3$ (30%, 700−900) catalysts. In all the samples, a broad desorption band was observed between 100 and 800 °C, which could be deconvoluted into three main peaks at about 250 (weak strength), 390 (medium strength), and 568 °C (high strength). In the cases of $KNO_3/Al_2O_3$ (30%, 700) and $KNO_3/Al_2O_3$ (30%, 900), the low =-temperature peak is more intense and the high temperature peak is less intense. However, in the TPD profile of $KNO_3/Al_2O_3$ (30%, 800), the peaks are stronger at both medium and high temperature (Table 3). In addition, using $CO_2$-TPD measurements, the amount of basic sites of the catalysts can also be evaluated, and the results are presented in Table 3. It can be seen from the table that $KNO_3/Al_2O_3$ (30%, 800) has the highest $CO_2$ adsorption volume, reaching 1.38 mmol/g, while $KNO_3/Al_2O_3$ (30%, 700) has the lowest. In the present work, it was observed that the catalytic activity of $KNO_3/Al_2O_3$ depended on not only the amount of basic sites but also their distribution. A high amount of basic sites, especially a high amount of medium-strength basic sites, is beneficial for GD synthesis. $KNO_3/Al_2O_3$ (30%, 800) has the maximum amount of basic sites and shows the highest GD yield (63.52%). For $KNO_3/Al_2O_3$ (30%, 900), although it has more basic sites than $KNO_3/Al_2O_3$ (30%, 700), its GD yield (39.71%) is lower than that of $KNO_3/Al_2O_3$ (30%, 700) (53.62%) (Table 1).

**3.2. Influence of Reaction Parameters.** The effects of several reaction parameters such as the temperature, the DMC/GL molar ratio, the catalyst amount, the reaction time, and the catalyst stability were studied for the transesterification of GL with DMC for the formation of GD.

*3.2.1. Effect of the Reaction Temperature.* To study the effect of temperature on the transesterification of GL with DMC, the reaction was performed at different temperatures varying from 50 to 70 °C while other reaction parameters such

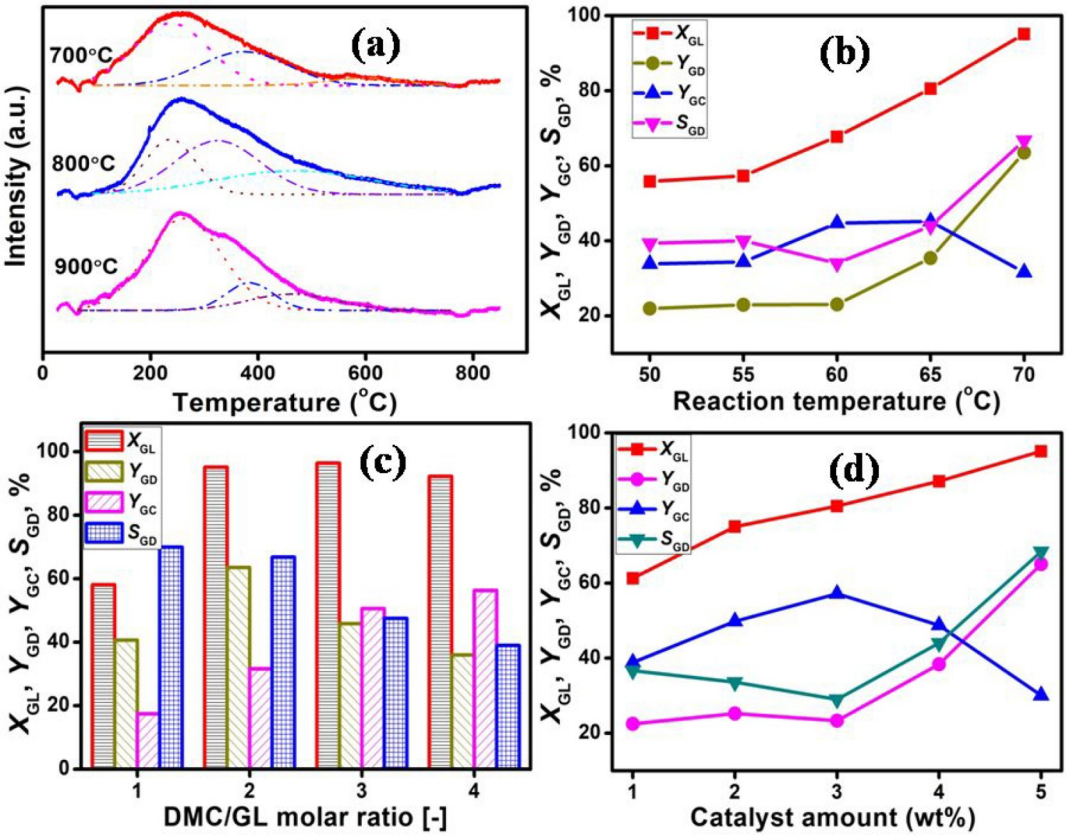


**Figure 5.** (a) $CO_2$-TPD profiles of $KNO_3/Al_2O_3$ with a 30% loading of $KNO_3$ at different calcination temperatures. (b) Effect of reaction temperature on the transesterification of GL with DMC. (c) The effect of the DMC/GL molar ratio on the transesterification of GL with DMC. (d) Effect of the catalyst amount on the transesterification of GL with DMC.



https://doi.org/10.1021/acsomega.2c02381
ACS Omega 2022, 7, 31778−31788

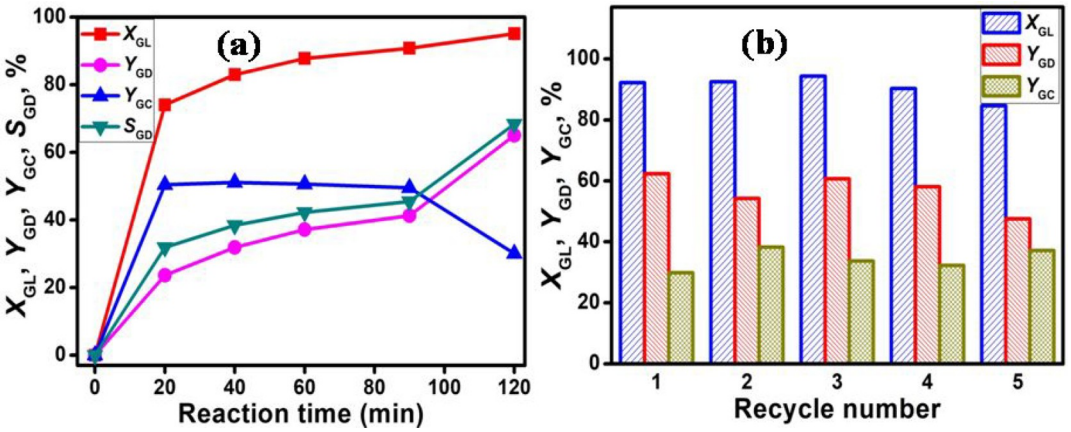


**Figure 6.** (a) Effect of the reaction time on the transesterification of GL with DMC. (b) Effect of the catalyst reusability on the transesterification of GL with DMC.

as the catalyst amount of 5 wt % (based on the GL weight), the reaction time of 120 min, and the DMC/GL molar ratio of 2:1 were kept constant. As shown in Figure 5b, when the reaction temperature was increased from 50 to 70 °C, the GL conversion and the GD yield increased slightly initially and then increased rapidly from 55.85% and 21.97% to 95.12% and 63.52%, respectively. The GD selectivity also increased with the reaction temperature. It was observed that both the transesterification of GL with DMC and the decomposition of GC were endothermic.[35] Thus, the high reaction temperature not only increased the reaction rate but also shifted the equilibrium to the product side; thus, both the GL conversion and the GD yield increased with the reaction temperature. Therefore, the optimum reaction temperature was set as 70 °C.

*3.2.2. Effect of the DMC/GL Molar Ratio.* Figure 5c shows the effect of the DMC/GL molar ratio on the transesterification of GL with DMC to produce GD. When the DMC/GL molar ratio was increased from 1 to 3, the GL conversion increased from 58.06% to 96.42%, respectively, while the GD yield increased from 40.61% to 45.83%. When the DMC/GL molar ratio was further increased to 4, the GL conversion decreased to 92.24% and the GD yield continued to decrease to 35.93%. Meanwhile, the GD selectivity decreased with the increase of the DMC/GL molar ratio. In addition, the GC yield increased from 17.45% to 56.31% when the DMC/GL molar ratio was increased from 1 to 4, respectively. These results showed that a higher DMC/GL molar ratio is adverse for the formation of GD. This is due to the fact that a higher DMC/GL molar ratio can shift the transesterification equilibrium to the right, resulting in increases in both the GL conversion and the amount of GC; thus, the instantaneous concentration of GC in the reaction zone would decrease due to the dilution effect.[33] Furthermore, as the DMC/GL molar ratio increases to 4, the instantaneous GC concentration in the reaction zone also decrease; thus, the transesterification rate becomes slow and the GL conversion and GD yield decrease. An overall analysis of the results indicated the 2:1 molar ratio as the optimized value for the reaction.

*3.2.3. Effect of the Catalyst Amount.* Figure 5d shows the effect of the catalyst amount on the transesterification of GL with DMC. When the catalyst amount increased from 1 to 5 wt %, the GL conversion and the GD yield increased from 61.31% and 22.49% to 95.12% and 63.52%, respectively. The GD selectivity initially decreased slightly from 36.68% to 28.99% and then increased to 66.78%. Meanwhile, the GC yield initially increased from 38.82% to 57.18% and then decreased to 31.6% when the catalyst amount increased from 1 to 5 wt %. For the transesterification of GL with DMC and the decomposition reaction of GC, increasing the catalyst amount increased the concentration of active sites in the reaction mixture, which resulted in an improved reaction rate and thus increased both the GL conversion and the GD yield. Therefore, 5 wt % was chosen as the opimum catalyst amount.

*3.2.4. Effect of the Reaction Time.* Figure 6a shows the effect of the reaction time on the transesterification of GL with DMC. During the initial 20 min, the reaction rate was high and the GL conversion rapidly reached to about 75%. Then, as the reaction time was increased to 120 min, the reaction rate decreased and the GL conversion also increased slowly to 95.12%. Meanwhile, GD and GC yields also increased rapidly during the initial 20 min. When the reaction time was increased to 90 min, the GD yield slowly increased to 41.29% and the GC yield remained almost constant at 50%. However, as the reaction time continued to increase to 120 min, the GD yield increased to 63.52% while the GC yield decreased to 31.6%. The GD selectivity also increased with the reaction time. A further increase in the reaction time had no effect on the GL conversion of the GD yield. Therefore, the optimum reaction time for the synthesis of GD was 120 min.

Lee and co-workers documented the synthesis of GD from the decomposition of GC and reported that the direct decomposition of GC needed to be carried out under relatively harsh conditions such as low pressure (∼ 2.7 kPa) and high temperature (150−250 °C).[36−38] However, in the one-pot synthesis of GD from the transesterification of GL with DMC described herein, the decomposition of GC took place under very moderate reaction conditions such as 70 °C, 120 min, and atmospheric pressure. It suggested that there might be some solvent effect coming into play in the one-pot synthesis. The decomposition of GC in the one-pot synthesis proceeded in a system containing GL, DMC, methanol, and a nanoparticulate catalyst which might have enhanced the decomposition of GC. In addition to the solvent effect, the developed catalyst has an obvious role in the conversion of GL, the decomposition of GC, and the formation of GD. The presence of strong basic sites in the catalyst might have accelerated the conversion of GL, the decomposition of GC, and the formation of GD.

**3.3. Catalyst Stability.** Recycling experiments were carried out to examine the stability of the $KNO_3/Al_2O_3$ (30%, 800)


https://doi.org/10.1021/acsomega.2c02381
ACS Omega 2022, 7, 31778−31788

catalyst. At first, the catalyst was separated by centrifugation, dried at 100 °C, and then reused directly in the next run. At the second recycling of the catalyst, it was found that the GL conversion slightly decreased to 85.78% but the GD yield remarkably decreased to 30.11%. At the fifth recycling of the catalyst, the GL conversion only reached to 48.07% and the GD yield was only 11.17% due to deactivation of the catalyst. To determine the reason for the decrease in the catalytic activity of the recovered $KNO_3/Al_2O_3$ (30%, 800) catalyst after the second recycle, the recycled catalyst was characterized by XRD and SEM. The SEM image showed a remarkable agglomeration of particles in the recovered catalyst. Figure 3d shows that the material phases of the recovered $KNO_3/Al_2O_3$ (30%, 800) are unchanged and that its main phases also contained $K_2O$, $Al_2O_3$, and $KAl_5O_8$ species. In addition, the potassium content of the product mixture after the first run was investigated using inductively coupled plasma (ICP), which showed mass concentration of only 0.0106%. The results indicated that the catalyst inactivation might be due to the leaching of active K species and a decrease in the surface area of the catalyst.[39] The potassium leaching is the main negative factor in the stability of the catalysts, as the catalyst surface becomes poisoned by new insoluble species (K aluminate) formed by the dissolution of $K_2O$ in the GL and methanol present in the reaction mixture. However, K aluminate species generate $K_2O$ active on the catalyst at higher temperature and thus the poisoning of catalyst is a slow process. Therefore, in the new recycling experiments, the $KNO_3/Al_2O_3$ (30%, 800) was calcined at 800 °C for 5 h after each run and then reused. The results are depicted in Figure 6b. At the fourth recycling of the catalyst, the GL conversion and the GD yield reached 90.32% and 58.08%, respectively. However, at the fifth recycling, the GL conversion and the GD yield slightly decreased to 84.67% and 47.56%, respectively. The results suggested that $KNO_3/Al_2O_3$ (30%, 800) was relatively stable and retained a high activity when reused four times after being calcined at 800 °C following the reactions.

**3.4. Proposed Reaction Mechanism.** Based on the results of characterizations and the catalytic activity experiments of $KNO_3/Al_2O_3$ nanoparticles, a plausible reaction mechanism for the one-pot synthesis of GD from the reaction of GL with DMC has been proposed. As shown in Scheme 2, in the first step of the reaction, the GL and DMC molecules are adsorbed on the active sites of the $KNO_3/Al_2O_3$ surface. In the second step, an acidic proton of the primary hydroxyl group (−OH) of adsorbed GL molecules is abstracted by the Lewis basic site ($O^{2-}$), resulting in the formation of activated $GL^-$. Meanwhile, the carbonyl oxygen of DMC interacts with the Lewis acidic site ($K^+$) of the catalyst, resulting in the activation of the carboxyl carbon of DMC. In the third step, the oxygen of the primary hydroxyl group of $GL^-$ causes a nucleophilic attack on the carbonyl carbon of DMC to form a methyl glyceryl carbonate intermediate, with the elimination of the methoxy group in the form of methanol. In the fourth step, the oxygen atom of the secondary hydroxyl group of GL intramolecularly attacks the nucleophilic carbonyl carbon of DMC to form GC, with loss of another molecule of methanol. In the fifth step, the Lewis basic site ($O^{2-}$) of the catalyst interacts with the alkenic carbon of GC to give a ring-opened intermediate. In the final (sixth) step, the ring-opened intermediate undergoes decarboxylation through an intramolecular nucleophilic substitution to form GD and $CO_2$. Meanwhile, the catalyst is regenerated. It can be observed that

**Scheme 2. Proposed Reaction Mechanism for the One-Pot Synthesis of GD from GL and DMC Using Nanocatalysts**

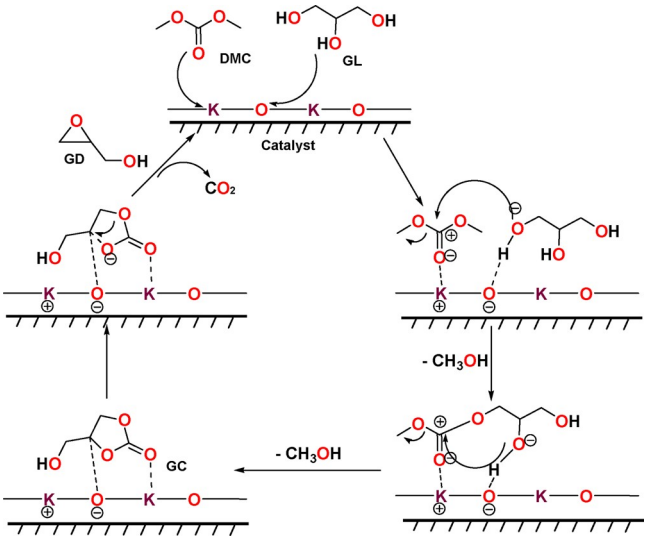


the basicity of the $KNO_3/Al_2O_3$ plays a crucial role in the reaction. The strong basic sites in $KNO_3/Al_2O_3$ accelerate the decarboxylation in the final step of the reaction.

**3.5. Comparison of the Catalytic Performance with Those of Previously Reported Catalysts.** To understand the efficiencies of $KNO_3/Al_2O_3$ solid base catalysts for the transesterification of GL with DMC for the synthesis of GD, efforts were made to compare the performances of the reported catalysts with those of solid base catalysts documented in the literature. Table 4 shows the DMC/GL molar ratio, catalyst amount (mol%), conversion yield of GL, reaction temperature, and moles of product formed per mole of catalyst used per hour for different catalysts in comparison to the $KNO_3/Al_2O_3$ catalyst. It can be seen from the table that $KNO_3/Al_2O_3$ demonstrated a comparable TOF and conversion yield of GL with a remarkably lower catalyst amount, DMC/GL molar ratio, and lower reaction temperature as compared to those of other catalytic systems. Overall, the comparison shows that $KNO_3/Al_2O_3$ is an efficient solid base catalyst for the transesterification of GL with DMC.

## 4. CONCLUSIONS

The work reported in this paper indicates that $KNO_3/Al_2O_3$ is an efficient solid base nanocatalyst for the one-pot synthesis of GD from GL and DMC. The preparation of the $KNO_3/Al_2O_3$ nanocatalyst involved an interaction between the $KNO_3$ phase and the $Al_2O_3$ support along with decomposition of $KNO_3$, which resulted in the formation of $KAl_5O_8$, the Al−O−K group and $K_2O$. The catalytic activity of $KNO_3/Al_2O_3$ depended on not only the proportion of basic sites but also their distribution. The solvent was envisioned to play a crucial role in the one-pot synthesis of GD. Overall, the one-pot synthesis is a facile route that affords excellent GL conversion and GD yield (~95% and 64%, respectively) over $KNO_3/Al_2O_3$(30%, 800) under moderate reaction conditions (DMC/GL molar ratio of 2:1, reaction time of 120 min, reaction temperature of 70 °C, and catalyst amount of 5 wt % based on the GL weight). Importantly, the developed catalyst can be reused four times without activity loss after being calcined at 800 °C.


https://doi.org/10.1021/acsomega.2c02381
ACS Omega 2022, 7, 31778−31788

Table 4. Performance Comparison of $KNO_3/Al_2O_3$ Catalyst with Other Solid Base Catalysts[a]

| catalyst | n(DMC/GL) | catalyst (mol %) | $X_{GL}$ (%) | T (°C) | time (h) | TOF[b] ($h^{-1}$) | ref |
|---|---|---|---|---|---|---|---|
| $K_2CO_3$/MgO | 2.5 | 1 wt % | 99 | 80 | 2 | 14.4[c] | 39 |
| NaOH/γ-$Al_2O_3$ | 2 | 6.9 | 97.9 | 78 | 1 | 14.0[c] | 40 |
| KF/$Al_2O_3$ | 2 | 5 wt % | 96 | 75 | 2 | 5.6[c] | 41 |
| NaOH-LF | 3 | 1.5 | 99.0 | 70 | 1.5 | 42.0[c] | 42 |
| $Na_2SiO_3$ | 4 | 18.8 | 96.7 | 95 | 0.25 | 20.2 | 43 |
| $Mg_4$Al-HT | 4 | 0.1 wt % | 32.9 | 80 | 2 | 18.9[c] | 44 |
| $KNO_3/Al_2O_3$ | 2 | 0.75 | 95.0 | 70 | 2 | 14.9[c] | present work |

[a]T, reaction temperature; time, reaction time; n(DMC/GL), DMC/GL molar ratio; and catalyst, catalyst amount (based on the amount of GL or the reactant). [b]TOF, moles of product per mole of catalyst per hour. [c]TOF calculated using the active materials.

## AUTHOR INFORMATION


### Corresponding Authors

**Mohd Imran** − *Department of Chemical Engineering, Faculty of Engineering, Jazan University, Jazan 45142, Saudi Arabia*; orcid.org/0000-0002-4815-9585; Email: imranchaudhary0@gmail.com

**Huajun Wang** − *Key Laboratory for Material Chemistry for Energy Conversion and Storage, Ministry of Education, School of Chemistry and Chemical Engineering, Huazhong University of Science and Technology, Wuhan 430074, P. R. China; Hubei Key Laboratory of Material Chemistry and Service Failure, School of Chemistry and Chemical Engineering, Huazhong University of Science and Technology, Wuhan 430074, PR China*; Email: wanghuajun@mail.hust.edu.cn

### Authors

**Elrasheed Elhaj** − *Key Laboratory for Material Chemistry for Energy Conversion and Storage, Ministry of Education, School of Chemistry and Chemical Engineering, Huazhong University of Science and Technology, Wuhan 430074, P. R. China; Chemical Engineering Department, Faculty of Engineering and Technical Studies, University of El Imam El Mahdi, Kusti 27711, Sudan*

**Salah Eldeen F Hegazi** − *Department of Chemical Engineering, Faculty of Engineering, Jazan University, Jazan 45142, Saudi Arabia*

**Mohamed Hassan** − *Department of Chemical Engineering, Faculty of Engineering, Jazan University, Jazan 45142, Saudi Arabia*

**Mubarak A Eldoma** − *Department of Chemical Engineering, Faculty of Engineering, Jazan University, Jazan 45142, Saudi Arabia*

**Jabir Hakami** − *Department of Physics, Faculty of Science, Jazan University, Jazan 45142, Saudi Arabia*

**Waseem A. Wani** − *Department of Chemistry, Government Degree College Tral, Kashmir, Jammu and Kashmir 192123, India*

**Anis Ahmad Chaudhary** − *Department of Biology, College of Science, Imam Mohammad Ibn Saud Islamic University (IMSIU), Riyadh 11623, Saudi Arabia*

Complete contact information is available at: https://pubs.acs.org/10.1021/acsomega.2c02381


### Notes

The authors declare no competing financial interest.

## ACKNOWLEDGMENTS

We acknowledge the financial support from the National Natural Science Foundation of China (NSFC) (21106050), the Specialized Research Fund for the Doctoral Program of Higher Education (SRFDP) (20100142120066), and the Fundamental Research Funds for the Central Universities of China (2015TS149). The authors are grateful to Analytical and Testing Center, Huazhong University of Science and Technology, for XRD and SEM analyses of the samples.

## REFERENCES


(1) Okoye, P. U.; Hameed, B. H. Review on recent progress in catalytic carboxylation and acetylation of glycerol as a byproduct of biodiesel production. *Renew Sustain Energy Rev.* **2016**, *53*, 558−574.

(2) Yusoff, M. H. M.; Abdullah, A. Z. Effects of zirconia loading in sulfated zirconia/SBA-15 on esterification of palmitic acid with glycerol. *Korean J. Chem. Eng.* **2018**, *35*, 383−393.

(3) Bagheri, S.; Julkapli, N. M.; Yehye, W. A. Catalytic conversion of biodiesel derived raw glycerol to value added products. *Renew Sustain Energy Rev.* **2015**, *41*, 113−127.

(4) Anitha, M.; Kamarudin, S. K.; Kofli, N. T. The potential of glycerol as a value-added commodity. *Chem. Eng. J.* **2016**, *295*, 119−130.

(5) Lee, H. J.; Shin, G. S.; Kim, Y. C. Characterization of supported Ni catalysts for aqueous-phase reforming of glycerol. *Korean J. Chem. Eng.* **2015**, *32*, 1267−1272.

(6) daCosta Evangelista, J. P.; Gondim, A. D.; Di Souza, L.; Araujo, A. S. Alumina-supported potassium compounds as heterogeneous catalysts for biodiesel production: A review. *Renew Sustain Energy Rev.* **2016**, *59*, 887−894.

(7) Vyas, A. P.; Subrahmanyam, N.; Patel, P. A. Production of biodiesel through transesterification of Jatropha oil using $KNO_3/Al_2O_3$ solid catalyst. *Fuel* **2009**, *88*, 625−628.

(8) Ochoa-Gómez, J. R.; Gómez-Jiménez-Aberasturi, O.; Maestro-Madurga, B.; Pesquera-Rodríguez, A.; Ramírez-López, C.; Lorenzo-Ibarreta, L.; Torrecilla-Soria, J.; Villarán-Velasco, M. C. Synthesis of glycerol carbonate from glycerol and dimethyl carbonate by transesterification: Catalyst screening and reaction optimization. *Appl. Catal. A Gen* **2009**, *366*, 315−324.

(9) Zhou, Y.; Ouyang, F.; Song, Z. B.; Yang, Z.; Tao, D.-J. Facile one-pot synthesis of glycidol from glycerol and dimethyl carbonate catalyzed by tetraethylammonium amino acid ionic liquids. *Catal. Commun.* **2015**, *66*, 25−29.

(10) Simanjuntak, F. S. H; Widyaya, V. T.; Kim, C. S.; Ahn, B. S.; Kim, Y. J.; Lee, H. Synthesis of glycerol carbonate from glycerol and dimethyl carbonate using magnesium − lanthanum mixed oxide catalyst. *Chem. Eng. Sci.* **2013**, *94*, 265−270.

(11) Bai, R.; Zhang, H.; Mei, F.; Wang, S.; Li, T.; Gu, Y.; Li, G. One-pot synthesis of glycidol from glycerol and dimethyl carbonate over a highly efficient and easily available solid catalyst $NaAlO_2$. *Green Chem.* **2013**, *15*, 2929−2934.

(12) Algoufi, Y. T.; Akpan, U. G.; Asif, M.; Hameed, B. H. One-pot synthesis of glycidol from glycerol and dimethyl carbonate over KF/sepiolite catalyst. *Appl. Catal. A Gen* **2014**, *487*, 181−188.

(13) Seiwert, J.; Leibig, D.; Kemmer-Jonas, U.; Bauer, M.; Perevyazko, I.; Preis, J.; Frey, H. Hyperbranched polyols via copolymerization of 1,2-butylene oxide and glycidol: comparison of

batch synthesis and slow monomer addition. *Macromolecules* **2016**, *49*, 38−47.
(14) Wu, P.; Tatsumi, T. A novel titanosilicate with MWW structure III. Highly efficient and selective production of glycidol through epoxidation of allyl alcohol with $H_2O_2$. *J. Catal.* **2003**, *214*, 317−326.
(15) Cespi, D.; Cucciniello, R.; Ricciardi, M.; Capacchione, C.; Vassura, I.; Passarini, F.; Proto, A. A simplified early stage assessment of process intensification: glycidol as a value-added product from epichlorohydrin industry wastes. *Green Chem.* **2016**, *18*, 4559−4570.
(16) Palomo, J. M.; Segura, R. L.; Mateo, C.; Terreni, M.; Guisan, J. M.; Fernández-Lafuente, R. Synthesis of enantiomerically pure glycidol via a fully enantioselective lipase-catalyzed resolution. *Tetrahedron: Asymmerty* **2005**, *16*, 869−874.
(17) Hanson, R. M. The synthetic methodology of nonracemic glycidol and related 2,3-epoxy alcohols. *Chem. Rev.* **1991**, *91*, 437−475.
(18) Pawar, A. A.; Chaugule, A. A.; Kim, H. Greener synthesis of dimethyl carbonate from carbon dioxide and methanol using a tunable ionic liquid catalyst. *Open Chem.* **2019**, *17*, 1252−1265.
(19) Garcia-Herrero, I.; Cuéllar-Franca, R. M.; Enriquez-Gutierrez, V. M.; Alvarez-Guerra, M.; Irabien, A.; Azapagic, A. Environmental assessment of dimethyl carbonate production: comparison of a novel electrosynthesis route utilizing $CO_2$ with a commercial oxidative carbonylation process. *ACS Sust Chem. & Engg* **2016**, *4*, 2088−2097.
(20) Gade, S. M.; Munshi, M. K.; Chherawalla, B. M.; Rane, V. H.; Kelkar, A. A. Synthesis of glycidol from glycerol and dimethyl carbonate using ionic liquid as a catalyst. *Catal. Commun.* **2012**, *27*, 184−188.
(21) Endah, Y. K.; Kim, M. S.; Choi, J.; Jae, J.; Lee, S. D.; Lee, H. Consecutive carbonylation and decarboxylation of glycerol with urea for the synthesis of glycidol via glycerol carbonate. *Catal. Today* **2017**, *293−294*, 136−141.
(22) Kondawar, S. E.; Patil, C. R.; Rode, C. V. Tandem synthesis of glycidol via transesterification of glycerol with DMC over Ba-mixed metal oxide catalysts. *ACS Sustainable Chem. Eng.* **2017**, *5*, 1763−1774.
(23) Lu, P.; Wang, H.; Hu, K. Synthesis of glycerol carbonate from glycerol and dimethyl carbonate over the extruded CaO-based catalyst. *Chem. Eng. J.* **2013**, *228*, 147−154.
(24) Elhaj, E.; Wang, H.; Gu, Y. Functionalized quaternary ammonium salt ionic liquids (FQAILs) as an economic and efficient catalyst for synthesis of glycerol carbonate from glycerol and dimethyl carbonate. *Mol. Catal.* **2019**, *468*, 19−28.
(25) Ahmed, M.; Sakthivel, A. Preparation of cyclic carbonate via cycloaddition of $CO_2$ on epoxide using amine-functionalized SAPO-34 as catalyst. *J. CO2 Util.* **2017**, *22*, 392−399.
(26) Anjali, K.; Christopher, J.; Sakthivel, A. Ruthenium-based macromolecules as potential catalysts in homogeneous and heterogeneous phases for the utilization of carbon dioxide. *ACS omega* **2019**, *4*, 13454−13464.
(27) Xie, W.; Peng, H.; Chen, L. Transesterification of soybean oil catalyzed by potassium loaded on alumina as a solid-base catalyst. *Appl. Catal. A Gen* **2006**, *300*, 67−74.
(28) Han, H.; Guan, Y. Synthesis of biodiesel from rapeseed oil using $K_2O/\gamma$-$Al_2O_3$ as nano-solid-base catalyst. *Wuhan Univ J. Nat. Sci.* **2009**, *14*, 75−79.
(29) Verziu, M.; Florea, M.; Simon, S.; Simon, V.; Filip, P.; Parvulescu, V. I.; Hardacre, C. Transesterification of vegetable oils on basic large mesoporous alumina supported alkaline fluorides-Evidences of the nature of the active site and catalytic performances. *J. Catal.* **2009**, *263*, 56−66.
(30) Yamaguchi, T.; Wang, Y.; Komatsu, M.; Ookawa, M. Preparation of new solid bases derived from supported metal nitrates and carbonates. *Catal. Surv from Japan* **2002**, *5*, 81−89.
(31) Sun, L.; Wu, Z.; Kou, J.; Chun, Y.; Wang, Y.; Zhu, J.; Zou, Z. Catalytic performance of supported $KNO_3$ solid bases for methylation of cyclopentadiene. *Chinese J. Catal* **2006**, *27*, 725−731.
(32) Zhu, J. H.; Wang, Y.; Chun, Y.; Wang, X. S. Dispersion of potassium nitrate and the resulting basicity on alumina and zeolite NaY. *J. Chem. Soc. Faraday Trans* **1998**, *94*, 1163−1169.
(33) Hu, K.; Wang, H.; Liu, Y.; Yang, C. $KNO_3$/CaO as cost-effective heterogeneous catalyst for the synthesis of glycerol carbonate from glycerol and dimethyl carbonate. *J. Ind. Eng. Chem.* **2015**, *28*, 334−343.
(34) Alonso, D. M.; Mariscal, R.; Moreno-Tost, R.; Poves, M. Z.; Granados, M. L. Potassium leaching during triglyceride trans-esterification using $K/\gamma$-$Al_2O_3$ catalysts. *Catal. Commun.* **2007**, *8*, 2074−2080.
(35) Li, J.; Wang, T. Chemical equilibrium of glycerol carbonate synthesis from glycerol. *J. Chem. Thermodyn* **2011**, *43*, 731−736.
(36) Lee, H. J.; Lee, S. D.; Ahn, B. S.; Kim, C. S.; Choi, J. S.Method for producing glycidol. US 8969600 B2, 2015.
(37) Choi, J. S.; Simanjuntak, F. S. H.; Oh, J. Y.; Lee, K. I.; Lee, S. D.; Cheong, M.; Kim, H. S.; Lee, H. Ionic-liquid-catalyzed decarboxylation of glycerol carbonate to glycidol. *J. Catal.* **2013**, *297*, 248−255.
(38) Ha, J. H.; Kim, J. S.; Kim, M. H.; Lee, K. Y.; Lee, M. S. Synthesis of glycidol by decarboxylation of glycerol carbonate over Zn−La catalysts with different molar ratio. *J. Nanosci Nanotechnol* **2016**, *16*, 10898−10902.
(39) Du, M. M.; Li, Q. X.; Dong, W.; Geng, T.; Jiang, Y. Synthesis of glycerol carbonate from glycerol and dimethyl carbonate catalyzed by $K_2CO_3$/MgO. *Res. Chem. Intermed.* **2012**, *38*, 1069−1077.
(40) Bai, R.; Wang, Y.; Wang, S.; Mei, F.; Li, T.; Li, G. Synthesis of glycerol carbonate from glycerol and dimethyl carbonate catalyzed by NaOH/$\gamma$-$Al_2O_3$. *Fuel proces technol* **2013**, *106*, 209−214.
(41) Sandesh, S.; Shanbhag, G. V.; Halgeri, A. B. Transesterification of glycerol to glycerol carbonate using KF/$Al_2O_3$ catalyst: The role of support and basicity. *Catal. lett* **2013**, *143*, 1226−1234.
(42) Okoye, P. U.; Abdullah, A. Z.; Hameed, B. H. Stabilized ladle furnace steel slag for glycerol carbonate synthesis via glycerol transesterification reaction with dimethyl carbonate. *Energy Conv Manag* **2017**, *133*, 477−485.
(43) Wang, S.; Xu, L.; Okoye, P. U.; Li, S.; Tian, C. Microwave-assisted transesterification of glycerol with dimethyl carbonate over sodium silicate catalyst in the sealed reaction system. *Energy Conv Manag* **2018**, *164*, 543−551.
(44) Devarajan, A.; Thiripuranthagan, S.; Radhakrishnan, R.; Kumaravel, S. Solvent free transesterification of glycerol into glycerol carbonate over nanostructured CaAl hydrotalcite catalyst. *J. Nanosci Nanotechnol* **2018**, *18*, 4588−4599.


https://doi.org/10.1021/acsomega.2c02381
*ACS Omega* 2022, 7, 31778−31788